RESEARCH ARTICLE | NOVEMBER 17 2014

Widely tunable room temperature semiconductor terahertz source

Q. Y. Lu; S. Slivken; N. Bandyopadhyay; Y. Bai; M. Razeghi

Appl. Phys. Lett. 105, 201102 (2014)
https://doi.org/10.1063/1.4902245
CHORUS

APPLIED PHYSICS LETTERS 105, 201102 (2014)

Widely tunable room temperature semiconductor terahertz source

Q. Y. Lu, S. Slivken, N. Bandyopadhyay, Y. Bai, and M. Razeghi[a)]
Center for Quantum Devices, Department of Electrical Engineering and Computer Science, Northwestern University, Evanston, Illinois 60208, USA

(Received 21 October 2014; accepted 10 November 2014; published online 17 November 2014)

We present a widely tunable, monolithic terahertz source based on intracavity difference frequency generation within a mid-infrared quantum cascade laser at room temperature. A three-section ridge waveguide laser design with two sampled grating sections and a distributed-Bragg section is used to achieve the terahertz (THz) frequency tuning. Room temperature single mode THz emission with a wide tunable frequency range of 2.6–4.2 THz (47% of the central frequency) and THz power up to 0.1 mW is demonstrated, making such device an ideal candidate for THz spectroscopy and sensing. [http://dx.doi.org/10.1063/1.4902245]

For most of the terahertz technology applications, a compact terahertz (THz) source emitting a wide frequency range (1–5 THz) is highly desired.[1] Example can be found in the spectroscopy and sensing, where many biochemical molecules have strong spectral fingerprints at terahertz frequencies,[2] and astronomical research, where a number of atomic and molecular emission lines in the THz range that are key diagnostic probes of the interstellar medium.[3] However, there are very few tunable THz sources with a compact size, and most of them have limited tuning ranges. Metal-oxide-semiconductor based THz sources are able to produce hundreds of lW of power at 0.32 THz with a narrow tuning of 10GHz.[4] Another example is the cryogenically cooled GaAs-based THz quantum cascade laser (QCL),[5] which can deliver a tuning range of 90GHz at 4.8THz with an external cavity,[6] or a continuous tuning range of 330GHz at 3.8 THz with a THz wire waveguide
coupled to a micro-electro-mechanical system.[7]

THz sources based on intracavity difference frequency generation (DFG) in mid-IR QCLs, on the other hand, are capable of room temperature continuous operation,[8] high power output power to mW level,[8] and wide frequency coverage.[9] These performance advancements have already made this technology attractive for applications in THz communication and imaging.[1] Besides, this type of THz source has been designed with a broad gain spectrum and a giant nonlinear susceptibility over a broad THz frequency range.[10] Lithographical step tuning from 1.0 to 4.6 THz is first demonstrated from an array of devices,[10] and recently enhanced to an even wider tuning from 1.2 to 5.9 THz with an external cavity.[9] Nevertheless, these tunable sources are complex systems, either consisting of several device components lasing at different frequencies or requiring extra movable optical setups. Fully monolithic tuning is also possible with this technology when using a dual-section laser with a standard distributed feedback grating design.[11] THz tuning from 3.44 to 4.02 THz is obtained by thermal tuning of the two sections with different electrical bias conditions.

Sampled grating (SG) design has been widely applied to the semiconductor lasers at telecom wavelengths to extend their monolithic tuning range.[12] Recently, SG distributed feedback (SGDFB)[13,14] or SG distributed-Bragg reflector (SGDBR)[15] designs have greatly enhanced the tuning range for a monolithic mid-IR QCL without using an external cavity. Continuous tuning of 50cm[1] in continuous wave operation[13] and step tuning of 236cm[1] in pulsed mode operation[14] at 4.8lm have been achieved. These are achieved with single frequency mid-IR QCLs. Here, we design and demonstrate the first room temperature, multi-section, twocolor SGDFB-DBR structure to realize a monolithic tunable THz source. A dual-section SG is used to tune one of the midIR wavelengths while a DBR section is used to secure the other wavelength. As such, wide frequency tuning from 2.6 to 4.2 THz with THz power ranging from 26 to 105lW is achieved at room temperature.

For THz sources based on DFG in a mid-IR QCL, the THz wavelength k_{THz} is determined by the two mid-IR wavelengths, k_1 and k_2 (defining $k_1 > k_2$), via $k_{THz} = 1/(1/k_2 - 1/k_1)$.[16,17] In order to tune the THz wavelength, the midIR wavelengths have to be controlled and tuned independently. Figure 1(a) shows the schematic of the three-section tunable THz device. It consists of a DBR section designed to control mid-IR wavelength k_1, and a dual SGDFB section for the tuning of mid-IR wavelength k_2. The DBR section has uniformly patterned grating lines, and the wavelength is determined by the grating period K_0. This section is electrically separated from the other sections and is biased with only DC current during the testing. Thus, the tuning relies on the change of the refractive index with the input electrical power. This tuning mechanism is quasi-continuous but with limited tuning range.

On the other hand, the SGDFB part comprises a series of short grating (grating period and number defined as K_g, N_g, respectively), periodically sampled on the front two sections of the device with two different sampling periods Z_1 and Z_2. The current injected into the front section is ideally independent of the current injected into the back section.

Unfortunately, the direct thermal tuning range of a uniform grating frequency is limited by the amount of injected electrical power, which hinders the potential for wider THz tuning.

Instead of a single reflectivity peak for each grating, the reflectivity becomes comblike, with multiple supermodes, as shown in Fig. 1(b). The total reflectivity plotted is seen from the center of a dual-section SG cavity with a DBR section attached to the back of the SG1 section. Supermode spacing (k_1, k_2) is inversely proportional to the sampling period, i.e., k_i ¼ 1=ð2n_{eff} Z_i d$K_g$$N_g$Þ. Here, n_{eff} is the modal refractive index, d is the effective refractive index difference between the unetched and the etched region of the grating, and i represents SG section numbers. k_1 and k_2 are designed with a slight difference, with k_1 <k_2, as shown in Fig. 1(c), such that the supermodes of each section overlap at only one wavelength within the tuning range Dk which is defined as

Dk ¼ $k_1$$k_2$=ð$k_2$ k_1Þ.

As the current in section SG1 (SG2) changes, the comb in this section shifts due to the changed modal refractive index, leading to a different supermode overlap in a step of k_2 (k_1). This is called the Vernier tuning mechanism. This shift is reflected in the THz frequency as well since the other mid-IR wavelength k_1 is secured by the DBR section. Continuous THz frequency tuning can be accomplished by either increasing or decreasing the current in both SG sections simultaneously.

A QCL wafer with a broadband dual-core active region optimized with large nonlinearities in the 1–5 THz range and CW operation when epi-down mounted is used for this work.[8]

a) Electronic mail: razeghi@eecs.northwestern.edu

0003-6951/2014/105(20)/201102/5/$30.00

A 500-nm InGaAs layer located 100nm above the laser core is used as the grating host layer. For SGDFB, both sections are sampled with a very short grating section (K_0 ¼1.3lm, N_g ¼13) for 7 times. The sampling periods Z_1 ¼270.4lm and Z_2 ¼245.7lm are used for the front and back sections, respectively. The estimated Vernier-only tuning range using the formula mentioned above is 62.7cm[1]. To enhance the power performance, the SG2 section is further elongated with a 1.5-mm unpatterned section for power amplification.

In this experiment, the SG reflectivity comb maximum is placed near the gain peak of the laser core, as shown in Fig. 1(b), to fully explore the SGDFB tuning range, while maintaining the DBR frequency at a position with a gain that is 75%–80% of the gain peak. To counterpoise the reduced gain at this position, the DBR section is designed with a large coupling strength. With a grating duty cycle around 50%, a grating length of 0.95mm, and a grating period of K_0 ¼1.474lm, the overall coupling coefficient (j) is 45cm[1] and the jL product is 4.5. Given a calculated intersubband absorption coefficient of 32cm[1] in the passive DBR section, the estimated reflectivity for k_1 is about 58%.

The wafer was processed into a double channel ridge waveguide having a width of W¼22lm, following the similar steps in Ref. 10. Additional electrical isolation channels were etched between the adjacent laser sections. These channels were etched 2.0lm deep through a 100lm wide mask into the InP cap and cladding layers. Experimentally, this provided a 600 X isolation measured near zero bias. After this, the sample was cleaved into 6.3mm long bars (containing a 1-mm DBR section, a 2-mm section for SG1, and a 3.3-mm section for SG2 and amplifying section), and AR coated with 1.1–lm Y_2O_3. The front facet was then polished at a 30 angle with respect to the cleavage plane for THz outcoupling. The device was epi-up mounted on a copper heat sink with indium solder for testing.

Mid-IR and THz power measurements were carried out on a thermoelectric cooler stage at 293K using a calibrated thermopile and Golay cell detector for power testing assuming 100% collection efficiency. Spectral measurements were performed with a Bruker Fourier transform infrared (FTIR) spectrometer equipped with uncooled mid-IR DTGS and farinfrared DTGS detectors for mid-IR and THz measurements, respectively. Due to the high current densities and epi-up mounting, the lasers had to be operated in pulsed mode, with the addition of DC biases to different sections to tune the laser frequency.[18] Thus, three independent drivers were used to inject the pulse/DC currents for spectral and power measurements.

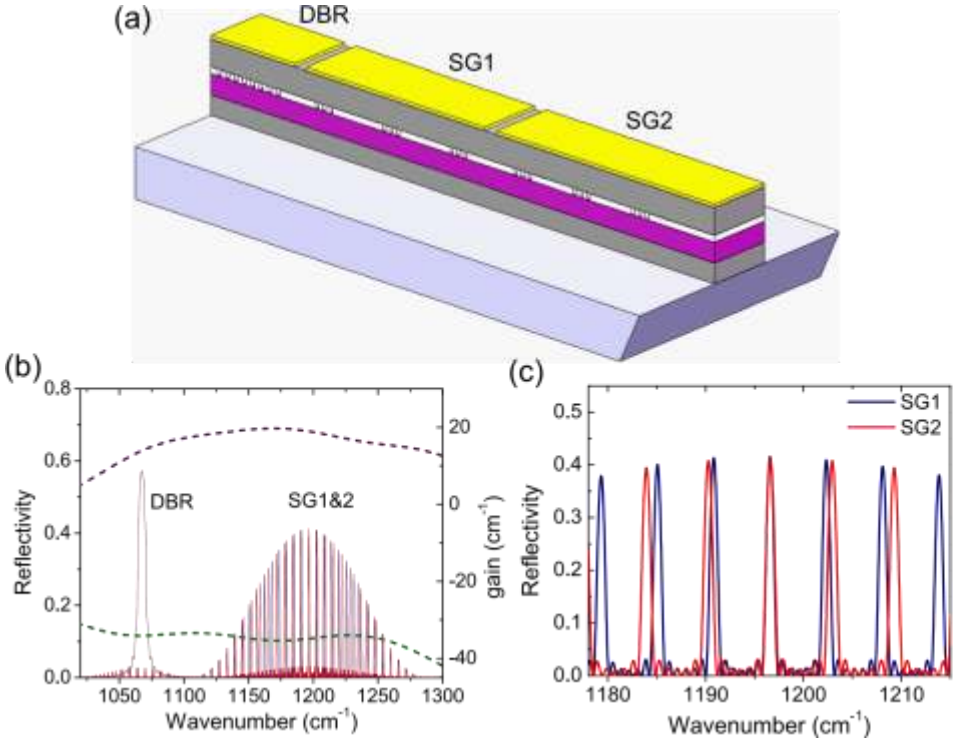

FIG. 1. (a) Schematic of the three-section device. (b) SGDFB and DBR reflectivity spectra corresponding to the calculated gain spectra at 0 V (green line) and 12 V (purple line) biases. (c) Detailed view of SGDFB reflectivity combs with the supermode spacings k_1, k_2 labelled.

The tuning behavior and characteristics of the mid-IR emission is shown in Fig. 2. Sections SG1 and SG2 are biased with pulsed currents of 3.8 A (1.52I_{th}) and 2.2A (1.46I_{th}), respectively (100-ns pulse width, 200-kHz repetition rate). All three sections are biased with independent DC currents for frequency tuning. The wide tuning for k_2 is realized mainly through Vernier tuning, in which the difference in DC currents for the two SG sections can be changed to rapidly hop between adjacent supermodes. The tuning for k_2 is from 8.24 to 8.63lm (1213.5 to 1158.5cm[1]), ranging 55cm[1]. The upper part of Fig. 2(a) (divided by a dashed line) is obtained by varying the DC currents on SG1, from 40mA to 290 mA with a step of 40–50 mA, while the lower part is obtained by varying the DC currents on SG2, from 40mA to 360mA with a step of 70–80mA, as shown in Figure 2(c). The average distances between the supermodes for the two parts are 5.75cm[1] and 5.25cm[1], respectively. Although the DBR section is individually biased at a constant DC current (50 mA), the corresponding wavelength k_1 is also slightly tuned, as shown

in Fig. 2(b), especially during the tuning of SG1 section, which results in a tuning range of 1.6cm^{1} for k_1 (Fig. 2(d)). This is because the significant heating during the DC current tuning of SG1 also affects the internal temperature of the adjacent DBR section.

The mid-IR total power for the two wavelengths, observed over the tuning range, is 1.32–1.58W, as shown in Fig. 3(a). This is compared with the maximum mid-IR power of 2.1W when the two SG sections are connected together and pumped with a single pulsed current driver with a duty cycle of 2%, as shown in Fig. 3(b). In this configuration, the device's threshold is 3.18kA/cm^{2}, and the laser shows stable dual-wavelength spectrum with a frequency spacing of 133cm^{1}, as shown in the inset of Fig. 3(b). The THz power

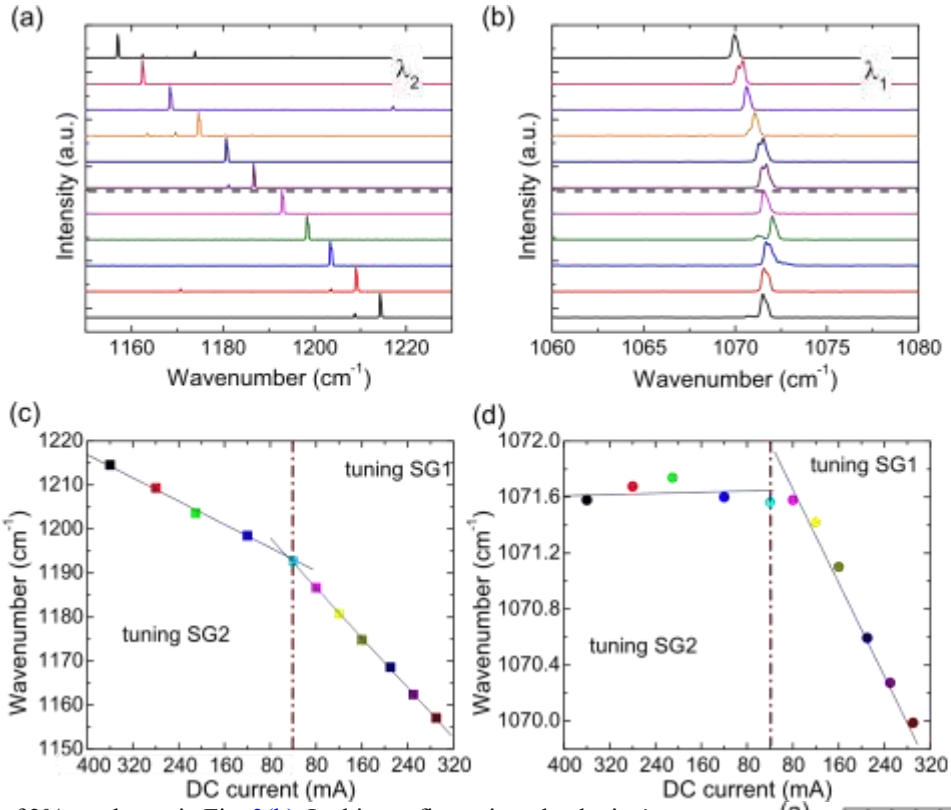

FIG. 2. (a) Vernier tuning of λ_2 as a function of wavenumber. (b) Slight tuning of λ_1 due to the current changes in the SG sections. Tuning of (c) λ_2 and (d) λ_1 as functions of DC currents on SG1 and SG2 sections.

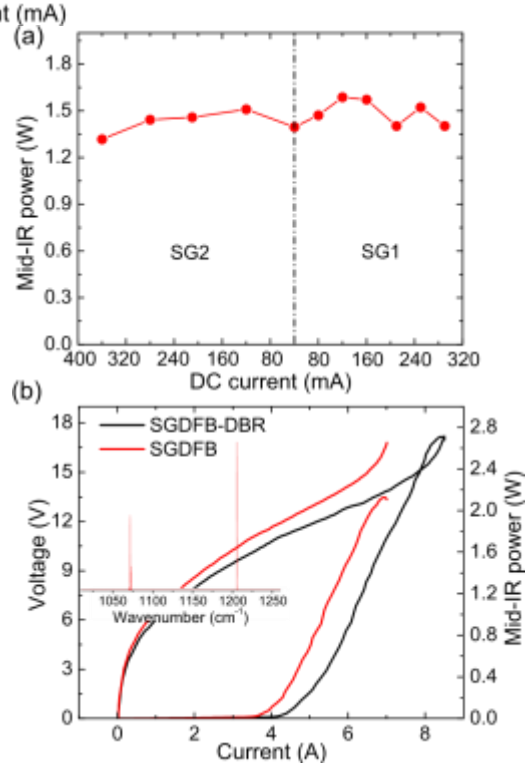

FIG. 3. (a) Mid-IR total peak power observed over the tuning range in response to DC current injection. (b) Power-voltage-current (P-I-V) characteristics of the three-section device when all sections are pumped together (black lines) with pulsed current and when only the SGDFB section is pumped (red lines). Inset: lasing spectra of the pumped SGDFB section at 6A.

of this device is 113lW at 4 THz with a conversion efficiency of 110lW/W^2. When all three sections are pumped together, the mid-IR power increases to 2.7W, with a threshold of 3.0kA/cm^2.

The measured THz tuning range and characteristics are shown in Fig. 4. A wide frequency tuning from 2.6 to 4.2THz with a step of 160–180GHz is achieved at room temperature by using the testing strategy for the mid-IR counterparts. This tuning range corresponds to 47% of the central THz frequency. In the tuned THz frequencies,
THz power ranges from 26 lW at 2.6 THz to 105 lW at 3.64THz. Since the mid-IR power (Fig. 3(a)) exhibits only a minor change in power during tuning, the THz power performance as a function of frequency is related mainly to the conversion efficiency characteristic of the device, as shown in Fig. 3(b). The conversion efficiency peaks around 3.2–3.8 THz and decreases towards the lower and higher frequency ends. Higher THz power and continuous wave operation can be further obtained by using a device structure with a higher THz conversion efficiency[2] and better thermal packaging.[19]

The above Vernier tuning mechanism is not continuous, with a step of 160–180GHz (5.36cm^{-1}) corresponding to the frequency spacing of the supermodes formed by the sampled gratings. However, the gaps can be bridged by varying the current in the DBR section to tune k_1, while the two SG sections are biased with small DC currents (i.e., 40mA). As shown in Figure 5(a), a total tuning range of 10cm^{-1} is achieved by changing the DC current from 50–550mA (corresponding voltage on DBR of V_{DBR} 4–9V). Note that the position of k_1 is determined by both the DBR section, and the SG sections, which act together as a resonator. Although there are some secondary peaks of the SG reflectivity combs near the DBR reflection peak for k_1, the intensity of the SG secondary peaks is only about 3% of the DBR reflection peak. Therefore, the present three-section device can be interpreted as a three-mirror device for k_1.[20] The modal spacing is determined by $D = 1/(2n_gL_{SG} + 2n_gL_{eff})$. Here, n_g is the waveguide group velocity, and L_{eff} is effective length of DBR section which is $L_{eff} = 1/(2j\tanh(jL_{DBR}))$. Given $j = 45cm^{-1}$, $n_g = 3.4$, $L_{SG} = 5.3mm$, and $L_{DBR} = 0.95mm$, DBR modal spacing $D = 0.274cm^{-1}$ is obtained. However, the DC current does have some minor impact on k_2, also shown in Fig. 5(a), which limits the accuracy of this technique alone. Better thermal isolation between the two sections should help reduce this effect.

Despite thermal crosstalk issues, truly continuous tuning of the THz frequency can be achieved by changing the DC currents on the SG sections 1 and 2 simultaneously in step of 40 and 70mA respectively, as shown in Fig. 5(b) (dashed lines). When combined with DBR current tuning, a range of 270GHz can continuously covered, as shown in Fig. 5(b). This tuning range is much wider than the Vernier tuning step (160–180GHz), and thus is sufficient to cover the gaps between supermodes. THz power varying from 81 to 68lW is observed during the tuning of the DBR. This power change is related to the heat generated in the DBR section which affects the SG sections and slightly decreases the mid-IR power.

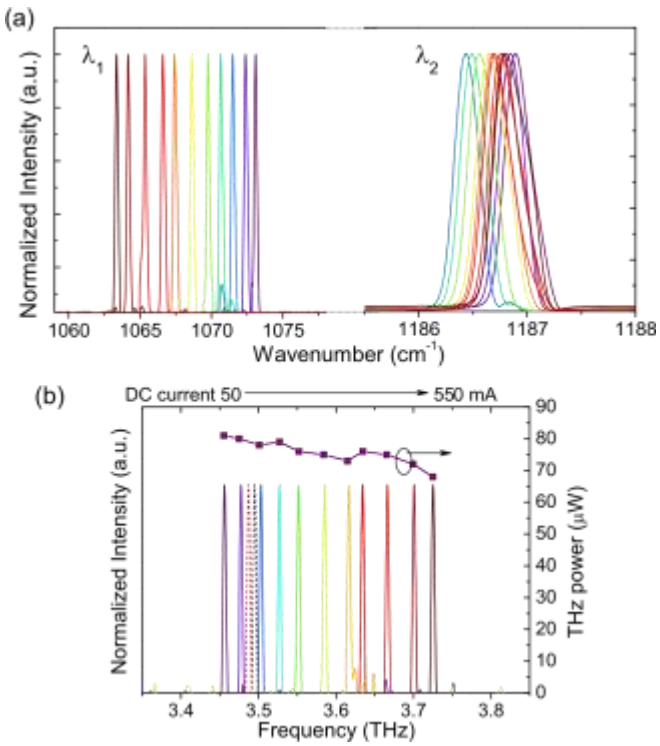

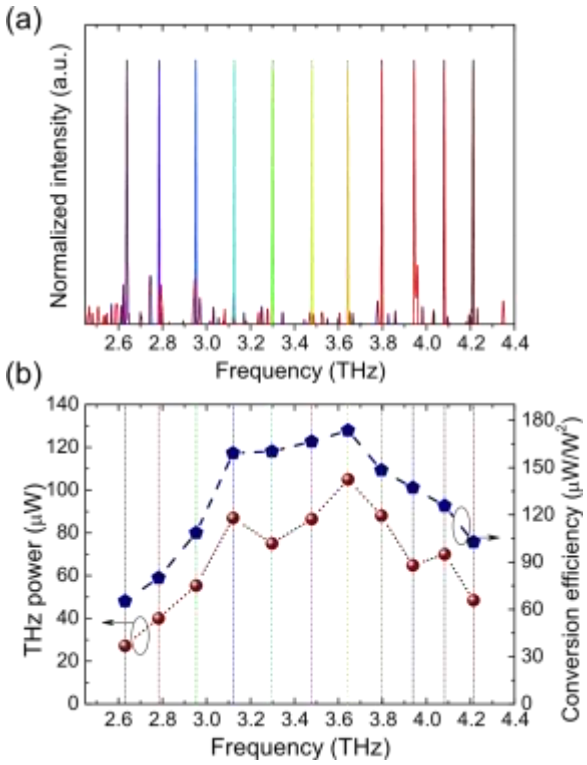

FIG. 4. (a) Combined THz spectra obtained via Vernier tuning mechanism. (b) THz power and conversion efficiency in the tuning range as a function of THz frequency.

FIG. 5. (b) Fine tuning of mid-IR k_1 by changing the DC current on the DBR section. Also shown is the slight tuning effect on k_2 due to the heat transfer from the DBR to the SG sections. (b) Corresponding THz fine tuning due to the tuning of k_1 and k_2. Dashed lines indicate the continuous tuning of THz frequency by changing the DC currents in SG sections simultaneously.

With further development, the THz continuous tuning range can be expanded. The DC power applied to the DBR section has not been maximized; the current range applied was only enough to bridge the current supermode gap. Given a typical break down voltage of 13V of our epi-up mounted device in DC mode, which corresponds to a DC current of 850–900mA and an injecting electric power of 11.5W, a DBR modal tuning of up to 600GHz ($20cm^{1}$) is achievable within the working current range. With a wider DBR modal tuning, the supermode spacing in the SG section can be increased to above $10cm^{1}$ by reducing the grating number N_g in one sampling period and decreasing the sampling period length Z_1 and Z_2. With this technique, the THz Vernier tuning range can be doubled up to 3.2 THz, which will enable the device to cover most of the 1–5 THz range.

In conclusion, we demonstrated a room temperature widely tunable monolithic THz source based on multisection SGDFB-DBR design in a mid-infrared quantum cascade laser. Single mode THz emission with a wide tunable frequency range of 2.6–4.2 THz is achieved with THz power up to 0.1 mW at room temperature. This dramatic increase in the tuning range compared any other electrically tunable THz source will lead to new opportunities for THz spectroscopy and sensing.

This work was partially supported by the National Science Foundation (Grant Nos. ECCS-1231289 and ECCS1306397), Department of Homeland Security (Grant No. HSHQDC-13-C-00034), Naval Air Systems Command (Grant No. N68936-13-C-0124), and an Early Stage Innovations Grant from NASA's Space Technology Research Grants Program. The authors would like to acknowledge the encouragement and support of all the involved program managers, and the useful discussion about three-driver system setup with Wenjia Zhou, Alexandre Godey, and Arnaud Janvier.

1 M. Tonouchi, Nat. Photonics 1, 97–105 (2007).
2 P. U. Jepsen, D. G. Cooke, and M. Koch, Laser Photonics Rev. 5, 124 (2011). 3 P. H. Siegel, IEEE Trans. Antennas Propag. 55, 2957 (2007).
4 Y. M. Tousi, V. Pourahmad, and E. Afshari, Phys. Rev. Lett. 108, 234101 (2012). 5 R. K€ohler, A. Tredicucci, F. Beltram, H. E. Beere, E. H. Linfield, A. G. Davies, D. A. Ritchie, R. C. Iotti, and F. Rossi, Nature 417, 156 (2002).
6 J. Xu, J. M. Hensley, D. B. Fenner, R. P. Green, L. Mahler, A. Tredicucci, M. G. Allen, F. Beltram, H. E. Beere, and D. A. Ritchie, Appl. Phys. Lett. 91, 121104 (2007).
7 Q. Qin, J. L. Reno, and Q. Hu, Opt. Lett. 36, 692 (2011).
8 Q. Y. Lu, N. Bandyopadhyay, S. Slivken, Y. Bai, and M. Razeghi, Appl. Phys. Lett. 104, 221105 (2014).
9 Y. Jiang, K. Vijayraghavan, S. Jung, F. Demmerle, G. Boehm, M. C. Amann, and M. A. Belkin, J. Opt. 16, 094002 (2014).
10 Q. Y. Lu, N. Bandyopadhyay, S. Slivken, Y. Bai, and M. Razeghi, Appl. Phys. Lett. 101, 251121 (2012).
11 S. Jung, A. Jiang, Y. Jiang, K. Vijayraghavan, X. Wang, M. Troccoli, and M. A. Belkin, Nat. Commun. 5, 4267 (2014).
12 V. Jayaraman, Z.-M. Chuang, and L. A. Coldren, IEEE J. Quantum Electron. 29, 1824 (1993).
13 S. Slivken, N. Bandyopadhyay, S. Tsao, S. Nida, Y. Bai, Q. Y. Lu, and M. Razeghi, Appl. Phys. Lett. 100, 261112 (2012).
14 T. S. Mansuripur, S. Menzel, R. Blanchard, L. Diehl, C. Pfl€ugl, Y. Huang, J.-H. Ryou, R. D. Dupuis, M. Loncar, and F. Capasso, Opt. Express 20, 23339 (2012).
15 S. Slivken, N. Bandyopadhyay, Y. Bai, Q. Y. Lu, and M. Razeghi, Appl. Phys. Lett. 103, 231110 (2013).
16 M. A. Belkin, F. Capasso, F. Xie, A. Belyanin, M. Fischer, A. Wittmann, and J. Faist, Appl. Phys. Lett. 92, 201101 (2008).
17 Q. Y. Lu, N. Bandyopadhyay, S. Slivken, Y. Bai, and M. Razeghi, Appl. Phys. Lett. 99, 131106 (2011).
18 S. Slivken, N. Bandyopadhyay, S. Tsao, S. Nida, Y. Bai, Q. Y. Lu, and M. Razeghi, Proc. SPIE 8631, 86310P (2013).
19 Q. Y. Lu, N. Bandyopadhyay, S. Slivken, Y. Bai, and M. Razeghi, Appl. Phys. Lett. 103, 011101 (2013).
20 L. A. Coldren and S. W. Corzine, Diode Lasers and Photonic Integrated Circuits (John Wiley & Sons, Inc., 1995).